Chemical Physics 515 (2018) 177–186

Contents lists available at ScienceDirect

Chemical Physics

journal homepage: www.elsevier.com/locate/chemphys

Adjacent keto and enol groups in photochemistry of a cyclic molecule: Products, mechanisms and dynamics

Dorit Shemesh[a], Ronnie Salomon[a], Stephanie Hyejin Kim[b], Geoffrey S. Tyndall[c], Sergey A. Nizkorodov[b], R. Benny Gerber[a,b,*]

[a] Institute of Chemistry and The Fritz Haber Research Center The Hebrew University, Jerusalem 91904, Israel
[b] Department of Chemistry, University of California, Irvine, CA 92697, USA
[c] National Center for Atmospheric Research, Boulder, CO 80301, USA

ARTICLE INFO

Keywords:
Photochemistry
1,2-Cyclohexanedione
2-Hydroxy-2-cyclohexen-1-one
Semi-empirical quantum-chemical potentials
Molecular dynamics for excited states
Reaction mechanisms

ABSTRACT

The photochemistry of carbonyl compounds is of considerable atmospheric importance, but the mechanisms and dynamics are often unknown. Here, we explore these topics for a system with adjacent keto and enol chromophoric groups. The photochemistry in the S_1 and S_2 states of the most stable tautomer of 1,2-cyclohexanedione, is studied theoretically using molecular dynamics simulations with a semi-empirical excited-state potential. Results are compared with experiments. The main results are: (1) Calculations provide an interpretation of the measured absorption spectrum. (2) There is good agreement between the predicted and experimental photoproducts. (3) Agreement with experiments on the products suggests the latter can be predicted without treating non-adiabatic transitions. (4) The mechanisms of formation of the products are predicted by the simulations. (5) The adjacent keto-enol system is found to be photochemically very different from the pure keto one.

1. Introduction

Interaction of light with matter is fundamental in naturally occurring processes such as photosynthesis [1], vision [2] and formation of vitamin D [3]. In many processes, the chromophore in which the electronic transition for a given spectral band is localized can be clearly defined. The localization of the excitation to a certain atom or a group of atoms in the molecule simplifies the understanding of the photochemical process. However, many other systems contain more than one chromophore, and therefore their photochemistry is far more complex. In this case, the interactions between the chromophores play an important role in treating the system: If the chromophores are sufficiently separated, then they can be treated individually, and a simpler picture arises. However, in the case of close proximity, the chromophores interact, and as a result, the photochemical processes of the combined chromophores may differ from the photochemistry of each individual chromophore [4,5]. The focus of this research is to get a better understanding of the strongly interacting chromophores.

One of the simplest and also widely found chromophores in nature is the carbonyl group. Carbonyl compounds are emitted to the atmosphere as a result of combustion processes and as secondary oxidation products of virtually all hydrocarbons [6–8]. Photoinduced processes in carbonyl compounds are important in atmospheric chemistry, as well as in organic chemistry, because carbonyls absorb solar radiation and have high quantum yields for certain photochemical reactions. For example, our recent study of the photochemistry of cyclohexanone has predicted rich photochemistry occurring on picosecond time scales following a photoexcitation in the first excited state [9].

In this paper we compare the photochemistry of cyclohexanone, containing one chromophoric carbonyl group, with a structurally related system, cyclohexanedione (CHD), containing two closely located chromophoric groups. Previous experimental studies relying on infrared spectroscopy in cold inert gas matrix environment [10], electron loss spectroscopy [11], ion cyclotron resonance mass spectrometry [12], electron diffraction spectroscopy [13] and NMR spectroscopy in solution [14] led to the conclusion that the diketo form of CHD is less stable than its keto-enol tautomer, i.e., 2-hydroxy-2-cyclohexen-1-one. Additionally, the stability of the keto-enol structure relative to the diketo-structure was confirmed by electronic structure calculations on different levels of theory [10]. In the following, we will abbreviate all tautomers of cyclohexanedione as CHD, but will add diketo or keto-enol modifiers for specifying the tautomer under discussion.

A previous experimental study of 253.7 nm (4.88 eV) photolysis of CHD in the gas phase [15] suggested the following mechanism. The

* Corresponding author at: Institute of Chemistry and The Fritz Haber Research Center The Hebrew University, Jerusalem 91904, Israel.
E-mail address: benny@fh.huji.ac.il (R.B. Gerber).

https://doi.org/10.1016/j.chemphys.2018.07.045

Available online 30 July 2018

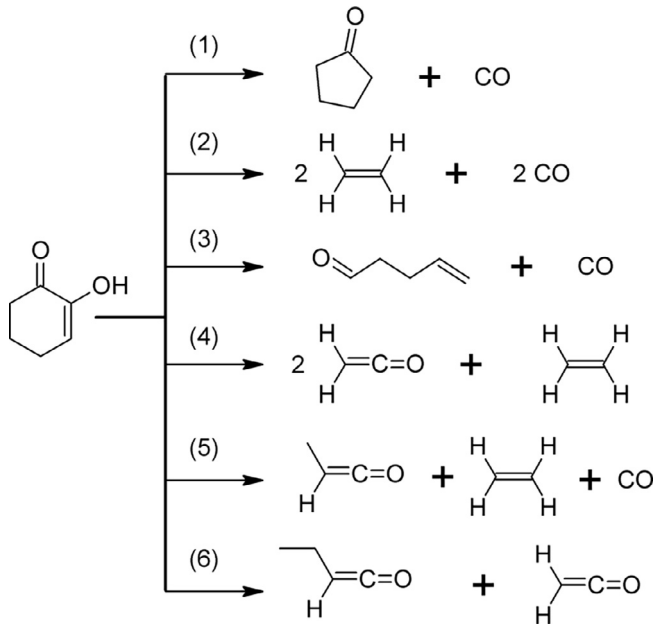

Scheme 1. Primary Photochemical Reaction Channels of CHD Proposed on the Basis of the Identified Photoproducts in the Study of Mukhopadhyay et al. [15].

system is initially excited to the second excited singlet state (S_2) due to its large oscillator strength at 253.7 nm (the band maximum is at 258 nm). The S_2 state is a bound state, therefore the system relaxes either to a triplet state or a lower lying singlet state and reaches then the ground state (S_0). Reactions are assumed to happen thermally on the S_0 state. Scheme 1 shows proposed photochemical reaction channels leading to the experimentally observed products.

Reactions 1 and 3 in Scheme 1 represent decarbonylation processes, resulting in carbon monoxide (MW = 28 g/mol) and cyclopentanone or 4-pentenal (both with MW = 84 g/mol), respectively. Reaction 2 produces two ethylene molecules (MW = 28 g/mol) together with two carbon monoxide molecules. Reaction 4 results in two ketene (MW = 42 g/mol) and one ethylene molecule. Reaction 5 creates methyl ketene (MW = 56 g/mol), carbon monoxide and ethylene. Reaction 6 gives ethyl ketene (MW = 70 g/mol) and ketene. As can be seen from Scheme 1, there are several alternative pathways for the same final products. For example, carbon monoxide is created in four different pathways, ethylene in three different pathways, and finally ketene is produced in two different pathways. It is therefore important to know the dynamics of the reaction to fully understand the mechanism of creation of each photoproduct. This information cannot be obtained from the experiment of Mukhopadhyay et al. [15], which relied on the final product analysis, but it can be obtained from a molecular dynamics simulation which follows the fate of an individual excited molecule. The statistics gathered from the analysis of a large number of molecular dynamics trajectories result in the yields for each pathway, which can then be compared to experimental findings to confirm or reject the proposed mechanism.

This study has two main objectives. Our first goal is to refine the mechanism of CHD photodissociation. The experimental study by Mukhopadhyay et al. [15] suggested that after photoexcitation and relaxation, the reactions occur on the S_0 state. In our study, we probe whether the reactions can occur also on the excited states, in competition with the internal conversion. To get a full mechanism of all possible photochemical processes, we are separately simulating excitation to the S_1 state or the S_2 state. Our second goal is to study photochemistry of CHD under atmospherically relevant conditions. While S_2 has the strongest absorption coefficient in the UV peaking at 260 nm, the weaker S_1 state is more accessible under conditions of the lower atmosphere. Photons with wavelength below 290 nm (4.3 eV) are efficiently absorbed by the ozone layer. We use simulations to contrast the photochemistry resulting from the S_1 and S_2 transitions. Since the S_1 state consists of a weak $n\pi^*$ transition, whereas the S_2 state is a strong $\pi\pi^*$ transition, the behavior of the molecule is expected to be different.

The paper is structured as follows. In section II, we discuss the systems and methods. In section III we report results and discussion. The results are divided into vertical excitation energy of the system, photoproducts obtained from simulation on the S_1 state, photoproducts obtained from simulation on the S_2 state, comparison to the single chromophore molecule cyclohexanone and a discussion whether internal conversion or intersystem crossing is important in this system. In section IV, we discuss the atmospheric implication of this study, and present our conclusions.

2. Systems and methods

2.1. 1,2-cyclohexanedione and 2-hydroxy-2-cyclohexen-1-one

Our previous work focused on photodissociation dynamics of cyclohexanone, one of the most common cyclic ketones [9]. Photoexcitation of the carbonyl group chromophore in this system was shown to lead to appearance of a range of photoproducts on a picosecond timescale. The aim of this work is to investigate the effect of a second chromophore on the photoexcitation dynamics. The simplest option is to add a second carbonyl group next to the first carbonyl group, resulting in 1,2-cyclohexanedione (CHD), as depicted in Scheme 2 on the left side. While cyclohexanone is considerably more stable in the keto form, CHD has two tautomers with comparable stability. Therefore, in addition to the diketo structure of CHD, Scheme 2 includes it keto-enol tautomeric form, 2-hydroxy-2-cyclohexen-1-one.

Fig. 1 shows the structures obtained from an MP2/cc-pVDZ level of calculation. The lowest energy tautomer is the enol tautomer, while the diketo structure is predicted to be higher in energy by 0.049 eV. Both structures are not planar, and adopt chair-like conformations. The keto-enol molecule gains stabilization compared to the diketo tautomer through a more effective π-π conjugation, and it is additionally stabilized with a hydrogen bond between the OH and the carbonyl group. With the energetic difference of 0.049 eV predicted at the MP2/cc-pVDZ level, the Boltzmann ratio between the tautomers is 0.14 at 300 K, strongly favoring the enol tautomer.

Experimental evidence supports the stability of the keto-enol structure in gas phase, low-pressure vapor, solvents and solid N_2 matrix [10,11,13]. A combined DFT and NMR study observed only the keto-enol structure in solution [14]. Using electron-loss spectroscopy in the gas phase, Francis et al. determined that CHD exist mainly in the keto-enol form [11]. Gas-phase electron diffraction on 1,2-cyclohexanedione at 295 K, combined with ab initio calculations, found the keto-enol form to be more stable [13]. Microwave measurements combined with MP2 calculations also support the predominance of the keto-enol form in the gas phase [16]. FTIR spectroscopy of CHD in low-pressure vapor, CCl_4 solution and solid N_2 matrix found almost solely the enol tautomer. Only in the pure solid CHD, the large dipole of the diketo form has a stabilizing effect, and the diketo form becomes preferred [10]. In view of the higher stability of the keto-enol form, the following discussion will be primarily focused on this tautomer.

Scheme 2. Tautomeric forms of 1,2-cyclohexanedione (CHD). The left structure is the less stable diketo form, 1,2-cyclohexanedione, the right structure is the more stable keto-enol form, 2-hydroxy-2-cyclohexen-1-one.

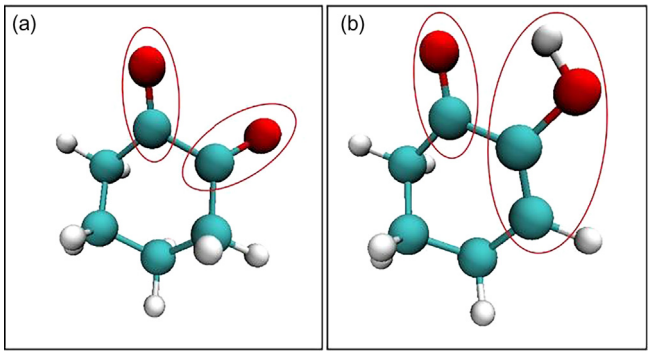

Fig. 1. MP2/cc-pVDZ optimized structures of (a) 1,2-cyclohexadione and (b) 2-hydroxy-2-cyclohexen-1-one (the enol tautomer of 1,2-cyclohexanedione). In both cases, the two chromophoric groups are encircled in red.

2.2. Theory

This study is closely related to our previous study on the photodissociation dynamics of cyclohexanone [9]. Although quantitative accuracy is not possible with the approach used in Ref. [9], the application of the same proven methodology to CHD should be able to semi-quantitatively predict major effects. We, therefore, will only briefly discuss the methodology, highlighting the essential differences, and refer the interested readers to our previous study for more details.

The simulation approach is based on two key ingredients: the potential energy surface and the dynamical description of the system. We first address the choice of the potential. Accurate potentials exist, such as CASPT2 [17], TD-DFT [18], MRCI [19], etc., that can be applied to energetic calculations on a system of this size. However, in a dynamical simulation, the energy calculations have to be carried out for each step of the simulation, which make these methods computationally expensive and not affordable for long time simulations and for the number of trajectories that are necessary for correctly predicting the product yields. Noteworthy are the recent advances in simulating short time processes (up to 1 ps) using CASPT2 gradients for systems of similar size to CHD [20,21]. In both studies, the relaxation to the ground state after photoexcitation, including the structural changes, were described on sub-picosecond timescales. However, as stated already, the purpose of our study is *to understand photochemical reactions that occur on longer timescales.* Those calculations are still not feasible using CASPT2 potentials on a timescale required to observe photochemical reactions. Based on our previous experience in studying the photochemistry of carbonyl compounds, we employed the orthogonalization-corrected method 2 (OM2) potential [22] for the ground state calculations and orthogonalization-corrected method 2/multireference configuration interaction (OM2/MRCI) potentials for the description of the excited states [23]. In previous studies, these potentials were proven to be reliable enough for treating photoexcitation processes [9,24–37]. Benchmarks studies show that the current OMx/MRCI methods perform reasonably well for many of the excited-state properties compared to methods like TDDFT/B3LYP, CC2, MRCISD and CASPT2 [38]. Our recent study on the photodissociation of acrylic acid [25], which compares the dynamics using these semi-empirical methods, with dynamics using the ADC(2) potential and with experiment, resulted in good agreement between the calculations and the experiments with respect to reaction mechanisms, photodissociation pathways, and yields of products. Thus, semiempirical potentials enable longer timescale simulations than ab initio potentials, including the description of complex photochemistry, such as different reaction mechanisms for products and their yields.

The second part of the methodology is the dynamical treatment of the system in the excited state. Many different approaches exist for treating the dynamical evolution on excited states as described in a recent review [39]. Examples of methods for treating excited states dynamics are multiple spawning [40], Tully's fewest switches algorithm [41] and non-adiabatic Car-Parrinello dynamics [42]. Recent developments include programs which facilitates the usage of a large variation of methods and potentials. SHARC is an example of a recently developed program that combines non-adiabatic dynamics with mainly ab initio potentials [43,44]. Applications of SHARC include the treatment of systems showing intersystem crossing, such as thymine [45] and 5-azacytosine [46], and recently 2-thiouracil in combination with the ADC(2) method [47]. Another program for treating non-adiabatic transitions in the excited states is JADE [48]. Recent work with JADE includes comparison of excited state dynamics using different potentials on keto isocytosine [49]. Noteworthy is also the work of Lan et al. in analyzing the huge amount of data created by molecular dynamics simulations using an approach from machine learning [50]. All these approaches have as a common basis an ab initio potential combined with different types of dynamical evolution. For the size of systems studied, these methods are able to describe short time dynamics (in the femtosecond to picosecond timescale) which applies to geometric distortion and relaxation from the initial excited state but not to chemical processes. In our approach, we are interested in chemical reaction dynamics, which take place on much longer timescales, and are therefore using a semi-empirical potential for reducing the computational costs of the simulation. We simulated photoexcitation to either the S_1 or S_2 excited state surfaces for reasons described above. The dynamics on each electronic state was treated adiabatically, i.e., state switching and intersystem crossings were not considered. While the potential energy surface was treated by quantum chemistry, the nuclear dynamics was treated classically by applying Newton's equation of motion using the OM2/MRCI potential energy surface [23]. The quantum potential energy surface can describe bond making and breaking. We have shown in our previous work on a number of carbonyl systems, that the photochemistry can be described reasonably well by considering dynamics on a single potential surface, therefore neglecting non-adiabatic transitions and intersystem crossing events. We therefore use the same approach here and assume that such events can be neglected. This is not to claim that crossing of potentials for different states do not occur, just to assume that only a small fraction of the reactive trajectories go through such crossings.

Ground-state minima were calculated using the OM2 methods and compared to the high-level MP2 method in conjunction with the resolution of identity (RI) approximation [51] using cc-pVDZ [52] as the basis set. The OM2/MRCI method was used for calculating excited state energies and properties. The active space was chosen to include the highest five occupied and the lowest five unoccupied orbitals. Three reference configurations were used for the MRCI calculations, namely closed-shell, singly excited, and doubly excited configurations involving HOMO and LUMO orbitals. The ab initio method ADC(2) [53] was used for validation for the excited-state properties of the semi-empirical method.

Sampling of the initial conditions was performed by running molecular dynamics simulation for 10 ps with a time step of 0.1 fs at 300 K using OM2 for the electronic ground state. Structures were chosen by applying two selection criteria to a large number of geometries obtained by the ground-state Born-Oppenheimer potential energy surface. First, the vertical excitation energy of the selected configuration to the first (or second) excited state lies in the range of ± 0.5 eV of the S_1 excitation (or S_2 excitation) of the reference geometry, the global minimum. In principle, excitation to all states is possible, but the energy window limits the excitation in this case to the first (or second) excited state only. Second, geometries were selected by considering their transition probability. The relative transition probability was calculated by using the oscillator strength, the energy gap, and the transition dipole moment (see reference [54] for more details). For each state, a random number $0 < n < 1$ was generated, and if n was smaller than the transition probability, then the structure was accepted. By this procedure, structures chosen as starting configurations on the S_1 or S_2

surface resulted in a significant number of 107 trajectories for the S_1 simulations and 205 trajectories for the S_2 simulations. As described above, the selection criteria depend on the energy and transition property of a specific state, therefore this procedure result in different starting geometries for each state. These numbers allow for reasonable statistical analysis of the different reactive events: Roughly speaking, events which occur with a weight of 1% in the results are likely to be represented in the trajectories.

The simulations were run for up to 100 ps with a time step of 0.1 fs. Some trajectories (14 on the S_1 and 94 on the S_2 surface) were discarded because of the energy conservation violation. Some trajectories (35 on S_1 and 74 S_2) were found to be unreactive. This resulted in a total of 56 S_1 reactive trajectories and 29 S_2 reactive trajectories during the 100 ps time window of the simulation. We have tried the adaptive timestep algorithm [55], which only improved the lengths of the trajectories slightly, but leaded to mainly non-reactive trajectories nevertheless. While the number of useful trajectories is lower for the S_2 surface, it is still large enough in order to ensure an appropriate sampling of the photochemistry.

Additionally, the absorption spectrum was calculated from a 100 ps long MD run on the ground electronic state using the OM2 potential. The long timescale of simulation enables a larger sampling of structures, and hence an improvement of accuracy in the calculated spectrum. A total of 10,000 geometries were extracted (one structure every 10 fs). Excitation energies and oscillator strengths for the first and second excited states were calculated. For each excitation energy, a Lorentzian (with a full width of 0.001 eV) was added to produce a smoothed spectrum. All of the Lorentzians were summed up to yield the excitation spectrum.

2.3. Experiment

The absorption cross section of CHD was measured in gas-phase and in organic solvents. For gas-phase measurements, solid CHD was volatilized in a 1-m pyrex gas cell fitted with quartz windows, to achieve a pressure ranging from 0.027 Torr to 0.077 Torr as measured with a Baratron pressure gauge (MKS model 227A). Radiation from a deuterium lamp was dispersed with an Instruments SA spectrometer with a resolution of 1 nm, and detected using an EG&G diode array detector [56]. Measured absorbances for 8 different trials were converted into absorption cross sections, and the results were averaged. For measurements in solution, CHD was weighed and dissolved in either ethanol or acetonitrile at different concentrations, and absorption spectra were taken with a dual-beam spectrophotometer (Shimadzu UV-2450). The measured absorbances were converted into cross-sections. Data below 250 nm were discarded for the acetonitrile solution because acetonitrile absorbs too strongly below this wavelength.

Photolysis of CHD was probed in gas phase using 253.7 nm mercury lamp. The photolysis was carried out in a smaller 0.6 L stainless steel vessel at 295 K at a CHD vapor pressure of 0.2 Torr. In some experiments, 600 few Torr of air was also added to the photolysis cell. Following the photolysis, the content of the photolysis chamber was transferred to a 47 L gas cell for analysis by FTIR for product analysis. Since all of the products detected by FTIR have already been detected in the Mukhopadhyay et al. [15] study, we elected to place our FTIR results in the supporting information section (see Figures S1-S4).

3. Results and discussion

3.1. Vertical excitation energies and absorption spectrum

Vertical excitation energies and properties of the keto-enol form of CHD calculated with ADC(2) are summarized in Table 1.

The first excited state at 4.03 eV is a weak nπ* transition, followed by a much stronger ππ* transition for the second excited state at 4.96 eV. The oscillator strengths are scaled to the strongest transition, in order to facilitate comparison between different structures and methods. There is a large difference between cyclohexanone, with one chromophoric group, and CHD with two chromophoric groups. In cyclohexanone, there is a large gap of about 3.5 eV between the first and the second excited state, specifically, the first state is at 4.19 eV (nπ* transition), and the second state is at 7.68 eV (ππ* transition). Therefore, the second excited state in cyclohexanone is too high in energy and not accessible for contributing to the excitation dynamics of cyclohexanone at the atmospherically relevant excitation energies (photons with energies above 4.3 eV cannot pass through the ozone layer).

In CHD, however, the second excited state is much lower in energy and might therefore contribute to the atmospheric photochemistry of CHD. The lowering of the S_2 state in CHD relative to that in cyclohexanone is from the more extensive conjugation across the π system that includes the carbonyl group, the C = C bond next to it, and the hydroxyl group, and makes the π-π* separation smaller. Under our experimental (excitation at 253.7 nm) and simulation (starting on either S_1 or S_2) conditions, both excited states should be accessible making it possible to examine the effect of the excited state in this system.

Furthermore, the differences in the molecular orbitals for the cyclohexanone and CHD are prominent: in the former the π and π* orbitals are located on the carbonyl group only, in the latter, due to the conjugation between the available π bonds, both orbitals are extended to the carbonyl and the enol group together. The n orbital in both systems are located mainly on the oxygen atom of the carbonyl group. The orbitals describing the nπ* and ππ* transitions are similar to those described by the study of Mukhopadhyay et al. [15]. The oscillator strength of the second excited state of ππ* character is several order of magnitudes larger than of the first excited state of nπ* character.

The OM2/MRCI vertical excitation energies of the keto-enol form of CHD are given for comparison in Table 2.

At the OM2/MRCI level of theory, both S_1 and S_2 are shifted down by about 0.25 eV compared to ADC(2). Still, the orbital excitations are the same for both states. Electron-impact spectroscopy localized the ππ* state at 4.84 eV [4], which is in excellent agreement with both methods, with ADC(2) predicting it at 4.96 eV and OM2/MRCI at 4.77 eV. The difference in the predictions for the third excited state (S_3) is larger, with the OM2/MRCI giving ~ 2 eV lower energy than ADC(2), but there is no experimental value available to compare to. Fortunately, only the first two excited states S_1 and S_2 are important for the dynamics; S_3 is much higher in energy and should therefore be not accessible under typical atmospheric conditions. The overall agreement is therefore reasonably good, and supports the usage of the OM2/MRCI method for the photoexcitation dynamics.

To highlight the effect of the second chromophore, one can compare the excitation energy of this compound, to the cyclohexanone in our

Table 1
Vertical excitation energy of 2-hydroxy-2-cyclohexen-1-one as calculated with ADC(2) method. Oscillator strengths are scaled to the strongest transition.

State	Energy (in eV)	Orbital transition	Description	Oscillator strength	Dipole moment (Debye)
S_1	4.03	HOMO-1 → LUMO 84 %	nπ*	0.0010	2.99
S_2	4.96	HOMO → LUMO 90 %	ππ*	1	5.92
S_3	7.32	HOMO-2 → LUMO 49 %		0.0015	3.73

Table 2
Vertical excitation energy of 2-hydroxy-2-cyclohexen-1-one as calculated with OM2/MRCI. Oscillator strengths are scaled to the strongest transition.

State	Energy (in eV)	Orbital transition	Description	Oscillator strength	Dipole moment (Debye)
S_1	3.75	HOMO - 1 → LUMO 85 %	nπ*	0.047	2.66
S_2	4.77	HOMO → LUMO 90 %	ππ*	1	4.43
S_3	5.48	HOMO → LUMO + 1 85 %		0.12	2.70

previous study. The excited states in cyclohexanone are of nπ* character or exhibit similarly a low oscillator strength. The effect of the enol group in CHD is to introduce a bright state of ππ* state in the accessible excitation range.

For comparison, the vertical excitation energies of the diketo form were calculated as well with ADC(2) and are given in Table 3.

Although, the predicted energies of the excited states are lowered compared to the corresponding energies for the keto-enol form, the transitions are all very weak, and have nπ* character (none of the bands can be described as ππ*). This makes the transition less likely to occur. Additionally, the Boltzmann distribution provides only a small contribution of this structure (a ratio of 0.14 was calculated between the diketo and the keto-enol form at room temperature). Therefore, it is reasonable to assume that the contribution of the diketo form to the photochemistry of this system can be neglected. Further evidence for the negligible contribution of the diketo structure comes from the predicted shape of the excitation spectrum, which is discussed in the following.

Fig. 2 shows the calculated spectrum compared to experimental spectra obtained in gas phase and in organic solutions. The spectrum displays considerably higher signal-to-noise than the spectrum of CHD reported by Mukhopadhyay et al. [15], enabling vibronic structure to be visible at the peak of the main band near 260 nm. The lower energy band near 320 nm is also clearly visible in the spectrum (Fig. 3).

The calculated major peak corresponding to the ππ* transition lies at ~275 nm, a smaller peak corresponding to the nπ* transition occurs at ~335 nm. The spectrum exhibits strongly the expected characteristics of keto-enol group. Our calculations suggest that the diketo structure does not contribute to the spectrum (no isomerization from the keto-enol form to the diketo form was detected in the simulations).

The experimental spectrum obtained in gas phase is similar in width, but blue shifted compared to the calculated spectrum. The maximum absorption lies around 260 nm, which fits extremely well to the previous study [15] which reports the maximum at 258 nm. A smaller peak in the experimental spectrum appears around 320 nm when the intensity is plotted on the log scale (Fig. 3). This peak can be attributed to the nπ* transition and its location is reasonably close to the theoretically predicted peak. We note that the relative intensity of the nπ* band is considerably higher when predicted by the OM2/MRCI method (relative S_1/S_2 oscillator strength 0.047, Table 2) as compared to the ADC(2) method (relative S_1/S_2 oscillator strength 0.001, Table 1). Comparison to the experimental spectrum suggests that OM2/MRCI may be overestimating the band strength for the S_1 transition relative to S_2. We also note that the hydroxyl group in keto-enol CHD affects the position of the ππ* band. Specifically, keto-enol CHD absorbs at longer wavelengths than methyl vinyl ketone (ππ* and nπ* bands at < 220 and 320 nm, respectively), which also has adjacent C=O and C=C bonds but no hydroxyl group.

The experimental spectra of CHD obtained in solution are of similar

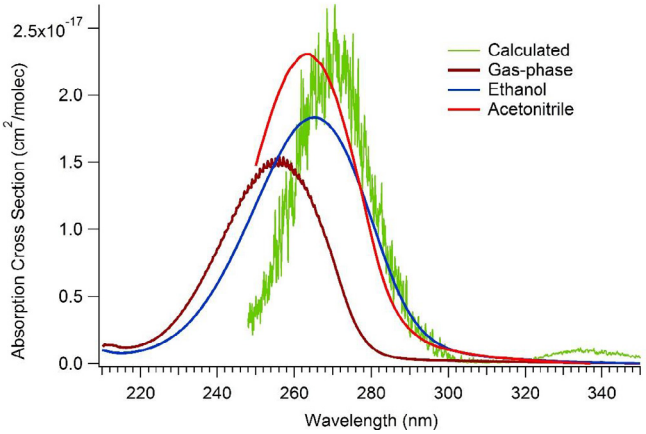

Fig. 2. Absorption spectra calculated with OM2/MRCI compared to experimental absorption spectra in gas phase, and in ethanol and acetonitrile.

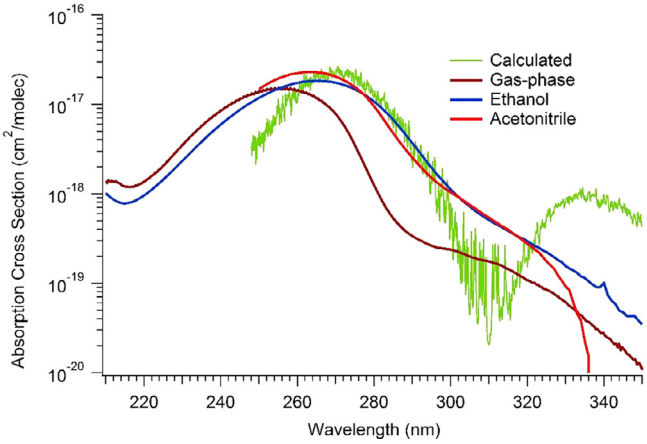

Fig. 3. Absorption spectra calculated with OM2/MRCI compared to experimental absorption spectra in gas phase, and in ethanol and acetonitrile. Absorption cross section is plotted on a log scale to emphasize the weaker nπ* band.

shape, but red- shifted compared to the gas-phase experimental spectrum. Also, the nπ* band is not as well defined in solution relative as it is in the gas phase (Fig. 3). The red-shift of the solution-phase spectra can be explained by the stronger solvent stabilization of the large dipole moment in the S_2 state of keto-enol CHD (5.92 D, Table 1) compared to that in the S_0 ground state (3.29 D). This shift of the ππ* band to the red is potentially important as it improves the overlap between the absorption cross sections and solar radiant flux density. This implies that CHD might be more photochemically active when it resides in a

Table 3
Vertical excitation energy of 1,2-cyclohexanedione as calculated with ADC(2). Oscillator strengths are scaled to the strongest transition in the keto-enol tautomer.

State	Energy (in eV)	Orbital transition	Description	Oscillator strength	Dipole moment (Debye)
S_1	2.97	HOMO → LUMO 90 %	nπ*	0.0001	4.08
S_2	4.21	HOMO - 1 → LUMO 60 %	nπ*	0.0001	3.19
S_3	5.93	HOMO → LUMO + 1 48 %	nπ*	0.0004	2.36

condensed phase (e.g., on environmental surfaces, in aerosol particles, or in cloud/fog droplets) compared to gas phase.

In summary, the comparison between the predicted and experimental absorption spectra strongly supports the keto-enol form of CHD, since only this tautomeric form would result in an intense ππ* peak in the spectrum. The predicted transitions of the diketo tautomer are very weak in absorbance, which, in combination with the low abundance of this tautomer, makes it difficult to detect.

3.2. Photochemical dynamics on S_1

3.2.1. Photoproducts

In this section, we will first summarize the statistics of the photoproducts of CHD and compare to the experimental yields. Qualitative comparison to the experiment is challenging because not all of the photoproducts are detectable by mass spectrometry. Likewise, FTIR spectroscopy can only detect a subset of products (e.g., only carbon monoxide and cyclopentanone could be positively identified in the FTIR spectra in Figures S1-S4). Therefore, the relative yields cannot be quantitatively determined from the available experimental data. We will have to compare the yields of the products on a qualitative basis only.

A key advantage of the theoretical approach is that timescales for different mechanisms can be obtained. In the following, we will therefore discuss in detail the main reaction pathways leading to these products, and describe the mechanisms and timescales.

Table 4 summarizes the product distribution of reactive trajectories on the S_1 state.

Most of the trajectories (47 out of 56 or 84%) include H transfer and H transfer back and resulted in the initial reactant, or an isomer of the reactant at the end of the 100 ps simulation. The isomer if the reactant is shown in Fig. 4. The isomer is obtained by H transfer from the hydroxyl group to the carbonyl group, resulting in a biradical.

In our simulation, we observed one or a combination of the following reactions: H transfer from the enol group to the carbonyl group (with and without back transfer), C–C cleavage between the carbon atoms bearing the functional group, cleavages of a different bond of the ring (minor pathway), resulting in ring opening and recombination of the fragment resulting in the reactant. In 4 out of 56 (7%) trajectories, we observed decarbonylation with formation of the enol isomer of cyclopentanone. The enol form of cyclopentanone obtained theoretically can be transformed into the keto form detected experimentally by an H transfer. We assume that the timescale of this process is longer than our simulation timescale and therefore we have not seen the keto form of cyclopentanone in our simulations. In the experiment, the formation of cyclopentanone could be verified by comparing the FTIR spectrum of the photolyzed reaction mixture to that of pure cyclopentanone vapor (FTIR spectra can be found in the supporting information section). An isomer of 4-pentenal is also obtained in the simulation, which happens to have the same molecular weight as cyclopentanone (84 Da) making it challenging to distinguish these two compounds by mass spectrometry (although Mukhopadhyay et al. [15] were tentatively able to tell them apart based on the fragment ions in electron impact mass spectra). The isomer of methyl ketene was obtained in 1 out of 56 (2%) of the trajectories. We will discuss its structure later when describing the reaction mechanisms. Eight out 56 (14%) trajectories resulted in a formation of CO. CO is the second main photoproduct, as can be seen also in the reaction scheme 1, which lists CO as a product in three different pathways. CO is also readily observed in the FTIR spectra, both in the work of Mukhopadhyay et al. [15] and in this work (Fig. S4). Finally, one out of 56 (2%) trajectories resulted in ethylene formation.

Comparing qualitatively the relative yields of our simulation to the experimental mass spectra, we see an overall good agreement. The simulation was not able to reproduce the experimental observation of ketene. Note, pathway 6 of scheme 1 predicts the creation of ethyl ketene (MW 70 Da) along with ketene (MW 42 Da). The peak at *m/z* 70 was observed in the mass spectra by Mukhopadhyay et al. [15], but its abundance did not change upon UV exposure. So the formation of ethyl ketene might be masked in the experiment by the fragment of the initial CHD reactant. Ketene was indeed observed experimentally. This opens the question, whether ketene is indeed obtained by pathway 6 or whether another mechanism yielding a different accompanying photoproduct is responsible for its formation.

Table 4
Product distribution obtained by theoretical simulation of the photoexcitation to the S_1 state.

Product	# of trajectories (out of 56)	Percentage	Nominal molecular weight (Da)
CHD (reactant or isomer of reactant)	47	84	112
Cyclopentanone or 4-pentenal	4	7	84
Isomer of methyl ketene	1	2	56
CO	8	14	28
Ethylene	1	2	28

3.2.2. Mechanisms and timescales of different photoproducts

3.2.2.1. Formation of cyclopentanone. Fig. 5 shows the time-sequence in which the enol form of cyclopentanone is created.

The initial geometry is the keto-enol form of CHD. At 1590 fs, an H atom is transferred from the hydroxyl group to the carbonyl group. After a short time, at 1810 fs, the C–C bond separating the two functional groups is cleaved. The system undergoes a structural rearrangement, yielding a linear structure at 2120 fs. After about 12 ps, the end segments of the intermediate approach each other, so that the system can form a five-membered ring instead of the previous 6-membered ring. This is followed by an almost immediate expulsion of a CO molecule. Note, that the simulation predicts the enol form of cyclopentanone. This form can be easily converted to the keto form by transferring the hydrogen of the hydroxyl group to the nearby carbon atom. The last step is not observed in our simulation presumably because it takes much longer than our simulation time. Indeed, in solution the ketonization of enols occurs on millisecond time scales (and is strongly pH dependent) [57]. Some of the pathways leading to the cyclopentanone product do not show the initial H transfer depicted in Fig. 5. The proposed mechanism fits well to the first reaction pathway in Scheme 1, in which cyclopentanone and carbon monoxide are created. In the study of Mukhopadhyay et al. [15], the same photoproduct is obtained on the ground state by a thermal dissociation pathway. However, the mechanism proposed by Mukhopadhyay et al. [15] is different in the order of the steps. In their mechanism, there is first a ring opening, followed by H transfer, then by CO detachment and finally by a ring closure.

3.2.2.2. Formation of ethylene. Three different pathways (namely pathway 2, 4 and 5) of Scheme 1 postulate ethylene formation. Pathway 2 results in ethylene and carbon monoxide, which can be also obtained by various different pathways. Therefore, it is an open question whether the system indeed proceeds through this pathway, or whether ethylene and carbon monoxide are obtained by other pathways. Pathway 4 is an additional mechanism for ethylene formation, since the by-product ketene has been confirmed experimentally. We were not able to find a trajectory describing pathway 4. Either the yield for this pathway is very low, or the simulation timescale is too short for observing this pathway. We only observe ethylene formation by pathway 5, see Fig. 6 for the mechanism, with a creation of an isomer of methyl ketene i.e. $C(OH)CHCH_2$ (a radical) instead of methyl ketene itself. The structure is depicted in Fig. 6 at step 2.

As can be seen from Fig. 6, two C–C bond of the ring are cleaved

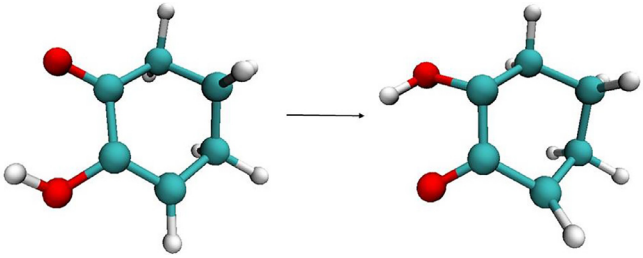

Fig. 4. H transfer from the hydroxyl group to the carbonyl group.

almost simultaneously. Approximately 40 fs later, a third C–C bond is cleaved, producing carbon monoxide, ethylene and an isomer of methyl ketene. Methyl ketene can be obtained by an H transfer from the hydroxyl group to the terminal carbon atom, presumably occurring on a longer time scale.

3.2.2.3. Formation of 4-pentenal. We observed the formation of an isomer of 4-pentenal, in agreement with pathway 3 in Scheme 1 (Fig. 7).

The creation of the isomer of 4-pentenal and carbon monoxide is happening within 200 fs from the start of C–C elongation. First, the C–C bond is elongated. When the C–C bond reaches the cleavage distance (2.5 Å), the adjacent C–C bond already starts to elongate. Finally, at 45.3 ps, the isomer of 4-pentenal and carbon monoxide are formed. 4-pentenal can be formed by the transfer of the H of the hydroxyl group to the adjacent carbon atom.

3.2.2.4. Formation of ketene. This product has not been seen theoretically, but found experimentally by Mukhopadhyay et al. [15]. Two pathways (pathway 4 and pathway 6) suggest creation of ketene. However, formation of ethyl ketene (pathway 6) could not be confirmed by the simulation and it also could not be unambiguously confirmed by mass spectrometry experiments. We therefore suggest that pathway 4 is the more likely route of ketene formation.

In summary, we have observed in our simulations the mechanisms for reaction pathways 1, 3 and 5 of Scheme 1. Reaction pathway 2 is possible, but the products can be also obtained by other pathways. Reaction pathway 4 is an appropriate mechanism for the formation of ketene (experimentally observed), since pathway 6 requires ethyl ketene as a by-product, which neither experiment nor theory predict.

3.3. Photochemical dynamics on S_2

The statistics of the photochemical reactions obtained after photoexcitation to the S_2 state is summarized in Table 5.

The reaction mechanisms leading to the photoproducts in the table appear to be similar to those occurring on the S_1 state, and are therefore not described here. The simulations on the S_2 state are more difficult to pursue due to problems in energy convergence and energy conservation. Therefore our statistics include only 29 trajectories, about half of number of trajectories simulated on the S_1 surface. The limited number of trajectories might therefore not represent all reaction pathways possible on the S_2 state. We nevertheless attempt to compare both simulations, keeping in mind the limited statistics on S_2. We see almost the same percentage of trajectories retaining the reactant or producing its isomer (47 out of 56) 84% on the S_1 state, to 83% (24 out of 29) of on the S_2 state. The sole reaction observed on the S_2 state is the decarbonylation into cyclopentanone and carbon monoxide. The yield of cyclopentanone is more than twice on the S_2 state than on the S_1 state. The yield of carbon monoxide is slightly different (14% on the S_1 state, 17% on the S_2 state). The results suggest that the same photochemistry happens on the S_2 state, but to a different extent. From our results, we conclude, that it would be difficult to distinguish photochemistry on these two states based solely on the photoproducts. Because there is no

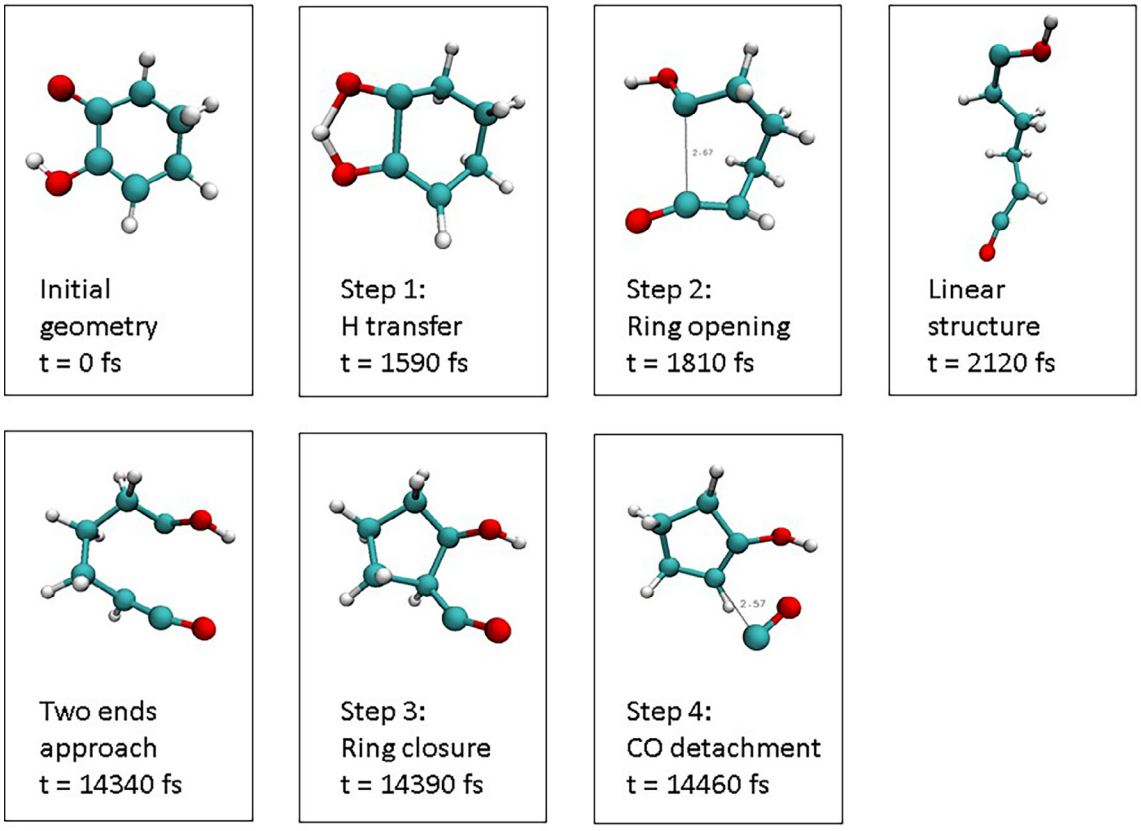

Fig. 5. Snapshots along a trajectory which shows the creation of the enol form of cyclopentanone and CO.

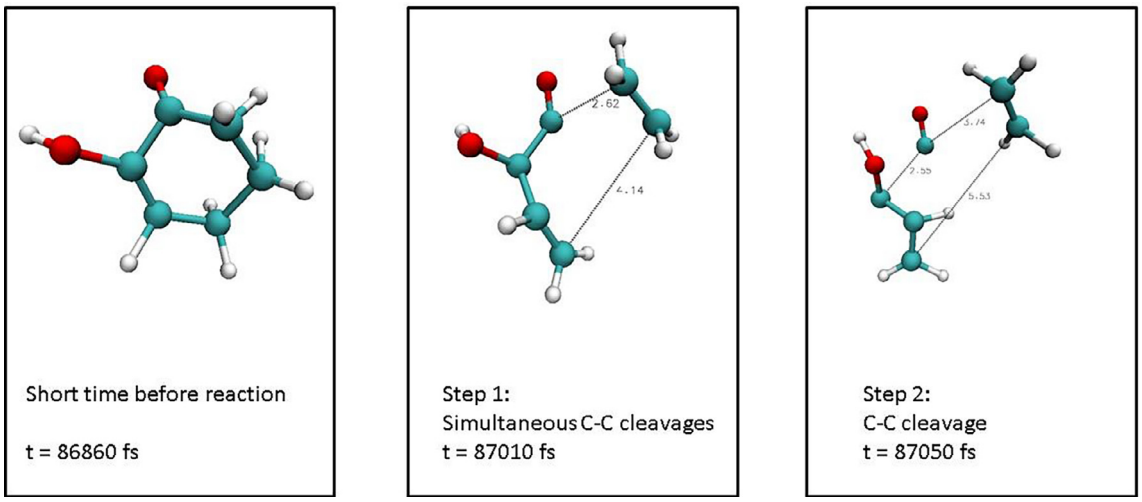

Fig. 6. Snapshots of a trajectory showing ethylene formation along with CO and an isomer of methyl ketene.

clear experimental marker that relates the photoproduct to one specific state, we assume that the first two excited states are contributing to the photochemistry of this system.

The study of Mukhopadhyay et al. [15] assumed that the system is excited to S_2 and then relaxes (either through S_1 or T_1) to the ground state S_0. Our work suggests that the internal conversion step to S_0 is not needed, and the same photochemical products can form on the S_1 or S_2 surfaces. We have not explicitly checked that the system does not relax to the ground state, but our results clearly show that the experimental photoproduct can be explained by doing simulations directly on the S_1 and S_2 states. Energy reaction profiles on the ground state were calculated for all photoproducts in the work of Mukhopadhyay et al. [15]. It is noteworthy, that their suggested mechanisms have certain steps in common with our prediction, such as ring opening and H transfer, however, the steps differ in the order of the occurrence. It is for example assumed, that first the open diketo structure is obtained, through steps involving ring opening and H transfer, and from this structure all photoproducts are created. In our simulations, we were not able to the see the creation of the diketo structure. Most of our isomers to the experimental observed structures are having a hydrogen atom connected to an oxygen atom. We assume that the H transfer occurs later. The difference between the mechanisms suggested by Mukhopadhyay et al. [15] and by ourselves may be due to different states that are involved (S_1 vs. S_0). We believe that the mechanistic details on different states might be similar, whereas the reaction barriers might differ. Our simulation has the advantage of being able to predict the order of the steps involved in a certain mechanism. It is noteworthy that the pathway creating ketene and ethylene has the highest barrier on the ground state. If we assume, that this is similar in the excited state, this might be a reason, why this pathway has not been observed.

3.4. Are triplets or conical intersections necessary?

In principle, both the calculation of Mukhopadhyay et al. [15] and the experiment of Walzl et al. [4] predict, that the T_1 state lies energetically close to the S_1 state and might therefore play a role in the photodissociation dynamics of this system. However, our simulations are in overall good agreement concerning yields and products with the experiment. We therefore believe, that at least some of the dynamics can be well described using the S_1 surface without having to invoke reactions on the T_1 surface. Given the large fraction of trajectories resulting in the reactant or its isomer, it is possible that the photoproducts not obtained in our simulations could be obtained over longer time scales by taking the T_1 state into account.

Additionally, our study shows that the photoproducts could be explained solely by assuming adiabatic dynamics on a single state, and that conical intersections may not be needed to describe the photodynamics of this system.

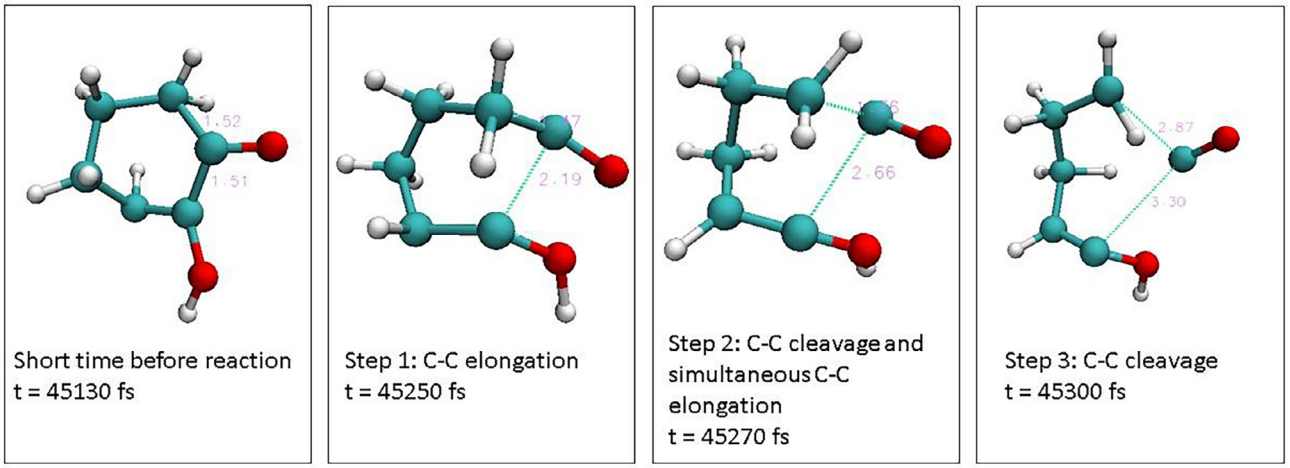

Fig. 7. Snapshots of the creation of an isomer of 4-pentenal and carbon monoxide.

Table 5
Product distribution obtained by theoretical simulation of the photoexcitation to the S_2 state. Since two products can be obtained by the same trajectory, the percentage sums up to more than 100%.

Product	# of trajectories (out of 29)	Percentage	Nominal molecular weight (Da)
CHD (reactant or isomer of reactant)	24	83	112
Cyclopentanone or 4-pentenal	5	17	84
Isomer of methyl ketene	0	0	56
CO	5	17	28
Ethylene	0	0	28

3.5. Comparison with photodissociation of cyclohexanone

There are significant differences in the photodissociation dynamics on the first excited state of cyclohexanone (containing one chromophore) and keto-enol CHD (containing two interacting chromophores). The most striking difference is in the number of reactive trajectories. In cyclohexanone, only about 8% of the trajectories were unreactive on the 100 ps time scale of the simulation, and the rest of the trajectories resulting in various reactions including ring-opening by cleaving the C-C_α bond, ring-opening followed by recombination, ring opening followed by CO detachment, ring opening followed by an H-atom transfer, and other processes. In contrast, the majority of the trajectories in keto-enol CHD produced no chemical change or an isomerization after 100 ps (Table 4). H-atom transfer occurs in CHD in about 84% of the trajectories, compared only to 17% in cyclohexanone. H-atom transfer is facilitated in the keto-enol form because the enol group is adjacent to the carbonyl group. This shows that both the S_1 and S_2 states of keto-enol CHD are considerably less reactive than the S_1 state of cyclohexanone. Of course, due to the time constraints on the length of the simulation, we cannot predict whether all excited states of keto-enol CHD eventually react on longer time scales or undergo intersystem crossing or internal conversion instead.

The major reactive pathway in cyclohexanone was the ring opening, accounting for more than 50% of the reactive trajectories. In keto-enol CHD, ring opening also occurs, but to a smaller extent – only 16% of the reactive trajectories show solely ring opening. The rest of the reactive pathways do not show a single C–C cleavage, but show rather several concerted or nearly simultaneous C–C cleavages. Decarbonylation pathways (i.e., loss of CO), either with or without ring closure, are both occurring in cyclohexanone and CHD. However, the percentage of decarbonylation is about twice as large (15% vs. 7%) for cyclohexanone compared to keto-enol CHD.

4. Concluding remarks and atmospheric implications

In this paper, we investigated theoretically and experimentally the photochemistry of CHD, a molecule with adjacent keto and enol groups. The study examined the photoabsorption into the S_1 and S_2 excited states, and of the reactions on the excited states. In addition, the results were used to compare the photochemistry of CHD with that of the previously studied, cyclohexanone, a cyclic ketone with a single chromophoric group.

The study of the absorption spectrum has shown that although two peaks of different intensities are observed in the absorption spectrum, the S_2 and S_1 absorption bands overlap quite strongly. The calculation show that photoabsorption is due to the keto-enol structure of the species, rather than to the diketo tautomer, and this is very much in accord with experimental data and predicted higher stability of the keto-enol form of CHD.

The photochemical reaction was investigated computationally by Molecular Dynamics simulations using potentials from a semi-empirical quantum chemical method. Comparison with experiment was made for the observed products. Detailed conclusions on the mechanisms of the reactions were extracted from the dynamics simulations. This leads to predictions of a substantial number of reaction channels, with a computed weight for each of these. It is encouraging that good agreement is found between the predictions of the photochemical dynamics on the major products, and the experimental observations. This inspires confidence that the mechanisms and reaction channels predicted by the Molecular Dynamics simulations are also likely to be correct. The computational efficiency of the semi-empirical quantum chemical method is a major advantage for future applications, also for photochemistry of much larger molecules.

However this must also be viewed with caution, and examined in future work. A recent study by two of the co-authors (D.S. and R.B.G.) on the photochemical dynamics of acrylic acid [25] compared the predictions of Molecular Dynamics with the semi-empirical potential with Molecular Dynamics using the ab initio ADC(2) method [53]. On the whole, good agreement was found between the two, especially in predictions of products. However, differences between significant details of the dynamics (e.g. timescales) were also found. We therefore conclude that further studies using ab initio Molecular Dynamics, however costly, may perhaps lead to improved version of the semi-empirical quantum chemical methods. This is also a major challenge to experiment in carrying out methods that can directly explore the mechanisms also for reactions as complex as studied here. Ultrafast time-resolved studies of the photochemical dynamics should greatly enhance knowledge of photochemical mechanisms and pathways.

This work has several important atmospheric chemistry implications. While the most common and most extensively studied atmospheric carbonyl compounds (such as acetone) contain a single chromophoric group, a number of more oxidized molecules found both in gaseous phase and in aerosol particles contain more than one functional group, and frequently contain adjacent chromophoric groups. The most abundant 1,2 dicarbonyls in the atmosphere are glyoxal and methyl glyoxal, which are produced by atmospheric oxidation of isoprene and aromatic compounds [58]. Larger 1,2-dicarbonyls, including cyclic ones, can be produced by a two-step oxidation of alkenes by OH (Scheme 3) or by OH oxidation of aliphatic ketones, as demonstrated in Ref. [59].

Compounds with adjacent carbonyl groups on a 6-membered ring, which are characteristic of the CHD structure, have been observed in products of ozonolysis of β-pinene [60] and sabinene [61]. Oxidation of polycyclic aromatic hydrocarbons such as pyrene and phenanthrene also results in 1,2-dicarbonyls on 6-membered rings, which were detected in the environmental samples [62]. The atmospheric fate of these 1,2-dicarbonyl compounds is poorly known. Our results suggest that these compounds should absorb solar radiation more efficiently because their electronic transitions are stronger and lower in energy compared to monocarbonyls. Based on our results, the photochemistry of these cyclic 1,2-dicarbonyls is quite different from photochemistry of the corresponding monocarbonyls. Furthermore, the bathochromic shift in the absorption spectrum in solution (Figs. 2 and 3) will further improve the overlap between the absorption spectrum and solar spectral flux density. This implies that 1,2-dicarbonyls compounds may be photochemically active not only in the gas phase but also in aerosol particles and liquid droplets. The photochemistry of 1,2-dicarbonyls should therefore be investigated in all phases to better understand the fate of these molecules in the atmospheric environment.

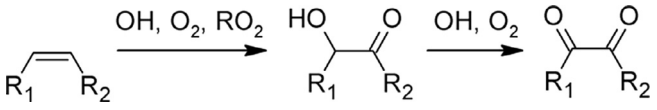

Scheme 3. Possible mechanism for production of 1,2-dicarbonyls in atmospheric oxidation of alkenes.

Acknowledgement

The National Center for Atmospheric Research is sponsored by the National Science Foundation. D.S. would like to thank Professor Domcke for his past mentorship in the framework of her PostDoc, during which time he introduced her to excited electronic states and photochemistry. R.S. acknowledges participation in the Alpha–Research Program, a joint initiative between the Future Scientists Center and the Ministry of Education, Department of Gifted and Talented High School Students (https://www.madaney.net/en/homepage).

Appendix A. Supplementary data

Supplementary data associated with this article can be found, in the online version, at https://doi.org/10.1016/j.chemphys.2018.07.045.

References

[1] R.E. Blankenship, Molecular Mechanisms of Photosynthesis, Wiley, 2004.
[2] A. Warshel, Nature 260 (1976) 679.
[3] E. Tapavicza, A.M. Meyer, F. Furche, Phys. Chem. Chem. Phys. 13 (2011) 20986.
[4] K.N. Walzl, I.M. Xavier, A. Kuppermann, J. Chem. Phys. 86 (1987) 6701.
[5] D. Dougherty, P. Brint, S.P. Mcglynn, J. Am. Chem. Soc. 100 (1978) 5597.
[6] P.B. Shepson, T.E. Kleindienst, E.O. Edney, C.M. Nero, L.T. Cupitt, L.D. Claxton, Environ. Sci. Technol. 20 (1986) 1008.
[7] E. Grosjean, D. Grosjean, M.P. Fraser, G.R. Cass, Environ. Sci. Technol. 30 (1996) 2687.
[8] C. George, M. Ammann, B. D'Anna, D.J. Donaldson, S.A. Nizkorodov, Chem. Rev. 115 (2015) 4218.
[9] D. Shemesh, S.A. Nizkorodov, R.B. Gerber, J. Phys. Chem. A 120 (2016) 7112.
[10] A.K. Samanta, P. Pandey, B. Bandyopadhyay, T. Chakraborty, J. Mol. Struct. 963 (2010) 234.
[11] J.T. Francis, A.P. Hitchcock, J. Phys. Chem.-Us. 98 (1994) 3650.
[12] G. Bouchoux, Y. Hoppilliard, R. Houriet, New. J. Chem. 11 (1987) 225.
[13] Q. Shen, M. Traetteberg, S. Samdal, J. Mol. Struct. 923 (2009) 94.
[14] D. Kubicki, A. Gryff-Keller, P. Szczecinski, J. Mol. Struct. 1021 (2012) 95.
[15] A. Mukhopadhyay, M. Mukherjee, A.K. Ghosh, T. Chakraborty, J. Phys. Chem. A 115 (2011) 7494.
[16] A.M. Pejlovas, M. Barfield, S.G. Kukolich, Chem. Phys. Lett. 613 (2014) 86.
[17] B.O. Roos, P. Linse, P.E.M. Siegbahn, M.R.A. Blomberg, Chem. Phys. 66 (1982) 197.
[18] E. Runge, E.K.U. Gross, Phys. Rev. Lett. 52 (1984) 997.
[19] H.J. Werner, P.J. Knowles, J. Chem. Phys. 89 (1988) 5803.
[20] J.W. Park, T. Shiozaki, J. Chem. Theory Comput. 13 (2017) 3676.
[21] L.H. Liu, J. Liu, T.J. Martinez, J. Phys. Chem. B 120 (2016) 1940.
[22] W. Weber, W. Thiel, Theor. Chem. Acc. 103 (2000) 495.
[23] A. Koslowski, M.E. Beck, W. Thiel, J. Computat. Chem. 24 (2003) 714.
[24] D. Shemesh, Z.G. Lan, R.B. Gerber, J. Phys. Chem. A 117 (2013) 11711.
[25] D. Shemesh, R.B. Gerber, J. Phys. Chem. Lett. 9 (2018) 527.
[26] D. Shemesh, R.B. Gerber, Adv. Chem. Phys. 159 (2016) 1.
[27] D. Shemesh, R.B. Gerber, Mol. Phys. 110 (2012) 605.
[28] D. Shemesh, S.L. Blair, S.A. Nizkorodov, R.B. Gerber, Phys. Chem. Chem. Phys. 16 (2014) 23861.
[29] D.E. Romonosky, L.Q. Nguyen, D. Shemesh, T.B. Nguyen, S.A. Epstein, D.B.C. Martin, C.D. Vanderwal, R.B. Gerber, S.A. Nizkorodov, Mol. Phys. 113 (2015) 2179.
[30] H. Lignell, S.A. Epstein, M.R. Marvin, D. Shemesh, R.B. Gerber, S. Nizkorodov, J. Phys. Chem. A 117 (2013) 12930.
[31] S.A. Epstein, D. Shemesh, V.T. Tran, S.A. Nizkorodov, R.B. Gerber, J. Phys. Chem. A 116 (2012) 6068.
[32] I. Dokukina, C.M. Marian, O. Weingart, Photochem. Photobiol. 93 (2017) 1345.
[33] Y.T. Wang, Y.J. Gao, Q. Wang, G.L. Cui, J. Phys. Chem. A 121 (2017) 793.
[34] B.B. Xie, S.H. Xia, X.P. Chang, G.L. Cui, Phys. Chem. Chem. Phys. 18 (2016) 403.
[35] D.P. Hu, J. Huang, Y. Xie, L. Yue, X.H. Zhuang, Z.G. Lan, Chem. Phys. 463 (2015) 95.
[36] L. Sporkel, J. Jankowska, W. Thiel, J. Phys. Chem. B 119 (2015) 2702.
[37] S.H. Xia, B.B. Xie, Q. Fang, G.L. Cui, W. Thiel, Phys. Chem. Chem. Phys. 17 (2015) 9687.
[38] D. Tuna, Y. Lu, A. Koslowski, W. Thiel, J. Chem. Theory Comput. 12 (2016) 4400.
[39] B.F.E. Curchod, T.J. Martinez, Chem. Rev. 118 (2018) 3305.
[40] M. Ben-Nun, J. Quenneville, T.J. Martinez, J. Phys. Chem. A 104 (2000) 5161.
[41] J.C. Tully, J. Chem. Phys. 93 (1990) 1061.
[42] N.L. Doltsinis, D. Marx, Phys. Rev. Lett. 88 (2002).
[43] M. Richter, P. Marquetand, J. Gonzalez-Vazquez, I. Sola, L. Gonzalez, J. Chem. Theory Comput. 7 (2011) 1253.
[44] S. Mai, P. Marquetand, L. Gonzalez, Int. J. Quantum Chem. 115 (2015) 1215.
[45] S. Mai, M. Richter, P. Marquetand, L. Gonzalez, Chem. Phys. 482 (2017) 9.
[46] A.C. Borin, S. Mai, P. Marquetand, L. Gonzalez, Phys. Chem. Chem. Phys. 19 (2017) 5888.
[47] S. Mai, F. Plasser, M. Pabst, F. Neese, A. Kohn, L. Gonzalez, J. Chem. Phys. 147 (2017).
[48] L.K. Du, Z.G. Lan, J. Chem. Theory Comput. 11 (2015) 1360.
[49] D.P. Hu, Y.F. Liu, A.L. Sobolewski, Z.G. Lan, Phys. Chem. Chem. Phys. 19 (2017) 19168.
[50] X.S. Li, Y. Xie, D.P. Hu, Z.G. Lan, J. Chem. Theory Comput. 13 (2017) 4611.
[51] F. Weigend, M. Haser, Theor. Chem. Acc. 97 (1997) 331.
[52] T.H. Dunning, J. Chem. Phys. 90 (1989) 1007.
[53] J. Schirmer, Phys. Rev. A 26 (1982) 2395.
[54] B.H. Bansden, C.J. Joachain, Physics of Atoms and Molecules, Longman, London, 1983.
[55] L. Sporkel, W. Thiel, J. Chem. Phys. 144 (2016).
[56] J.J. Orlando, G.S. Tyndall, J.M. Fracheboud, E.G. Estupinan, S. Haberkorn, A. Zimmer, Atmos. Environ. 33 (1999) 1621.
[57] J.R. Keeffe, A.J. Kresge, N.P. Schepp, J. Am. Chem. Soc. 112 (1990) 4862.
[58] T.M. Fu, D.J. Jacob, F. Wittrock, J.P. Burrows, M. Vrekoussis, D.K. Henze, J. Geophys. Res-Atmos. 113 (2008).
[59] J.D. Crounse, L.B. Nielsen, S. Jorgensen, H.G. Kjaergaard, P.O. Wennberg, J. Phys. Chem. Lett. 4 (2013) 3513.
[60] M. Jaoui, R.M. Kamens, J. Atmos. Chem. 45 (2003) 101.
[61] L.Y. Wang, L.M. Wang, Phys. Chem. Chem. Phys. 19 (2017) 24209.
[62] R.E. Cochran, I.P. Smoliakova, A. Kubatova, Int. J. Mass. Spectrom. 397 (2016) 6.